https://doi.org/10.5194/egusphere-2026-1626
Preprint. Discussion started: 15 April 2026

Movement history of faults under variable stress fields – insights derived from 3D seismics in the central northern Upper Rhine Graben, Germany

Sonu Roy[1], Johannes Mair[1], David C. Tanner[2], Ariane Djahansouzi[3], and Andreas Henk[1]

[1]Technical University of Darmstadt, Schnittspahnstraße 9, D-64287 Darmstadt, Germany
[2]LIAG Institute for Applied Geophysics, Stilleweg 2, D-30655 Hannover, Germany
[3]Landkreis Darmstadt-Dieburg, Abteilung Klimaschutz, Infrastruktur, Standortförderung, Jägertorstraße 207, 64289 Darmstadt, Germany

Correspondence: Sonu Roy (roy@geo.tu-darmstadt.de)

Abstract. The tectonic history of the Upper Rhine Graben (URG) is still unclear, despite decades of research. This is because of the lack of good quality 3-D seismic data to investigate the subsurface. We reconstruct the tectonic evolution of the central northern Upper Rhine Graben (NURG) by analyzing a 3D seismic survey that covers approximately 300 km^2 between Worms in Rhineland-Palatinate and Darmstadt in Hesse, Germany.

We aim to understand the interactions between the faults, the sedimentation pattern near the fault areas, their evolution in relation to the major structures of the URG, and to deduce the associated stress regime. Seven of the largest normal faults were selected (five strike NNW–SSE and two strike WNW–ESE), and the sediment thickness maps in each stratigraphic zone were generated using interpreted seismic horizons. Based on the thickness maps and the syn-sedimentary fault activity, the normalized Expansion Index (EI) was calculated. The analysis indicates that NNW–SSE fault activity was dominant pre-24 Ma, while the fault activity of WNW–ESE faults became more prominent post-24 Ma. Independent structural evidence, including the geometrical refraction of fault intersection traces (attributed to the reactivation of inherited Variscan basement trends) and the unilateral southward migration of displacement maxima, physically documents the rotation from E-W extension to NW-SE transtension. We postulate that all seven faults are active to the present day, as they can be traced seismically to the near surface. Recently acquired geophysical data (including shear-wave seismics) by our research group confirms recent activity on two of these faults.

We conclude, based on the seismic interpretation of our study area and the derived results, that URG underwent through two distinct tectonic phases: 1) a pre-24 Ma rifting stage and 2) a post-24 Ma transtensional stage that has lasted to the present-day. This finding aligns with other recent studies on the tectonic evolution of the URG. Rift systems evolving under variable stress regimes can develop complex fault architectures as changing stress orientations reactivate inherited structures and redistribute strain through time. Our results show that such stress-field changes can transform initially simple extensional fault systems into more segmented and interacting networks, where older rift faults and newly activated transfer structures jointly control fault propagation, basin subsidence, and sedimentation patterns.

1 Introduction

The Upper Rhine Graben (URG) is a prominent part of the European Cenozoic Rift System (ECRIS), which extends from the western Mediterranean Sea to the southern North Sea (Ziegler, 1992; Dèzes et al., 2004). Subsidence of the URG started in Eocene times and continues, interrupted by phases of non-deposition and erosion, until the present day (Sissingh, 2003). The current active tectonic setting of the approximately 300 km long URG is documented by earthquake activity as well as by uplift of the rift shoulders and subsidence of the basin floor (Dèzes et al., 2004; Cardozo and Behrmann, 2006b). The rift basin is characterized by a complex network of faults that has not only played a pivotal role in its formation but is also relevant for ongoing geothermal exploration (Beccaletto et al., 2010), among other things. Various hypotheses, ranging from a rather uniform to a multi-stage geodynamic evolution, involving significant temporal variations in the orientation and magnitude of the regional stress field since Eocene times, have been put forward to explain the preserved sedimentary record as well as spatial variations in uplift and subsidence patterns (Schumacher, 2002a; Rotstein et al., 2005; Cardozo and Behrmann, 2006b).

A Quaternary sediment cover fills the graben, rendering outcrops of Paleogene to Neogene age rare. Therefore, geophysical approaches are the methods of choice when attempting to image the subsurface of the URG. Valuable information about paleo-stress orientations and tectonic regimes is recorded by syn-sedimentary fault activity and by lateral thickness variations of individual stratigraphic units. However, borehole and 2D seismic data can only provide an incomplete picture of the interplay between fault activity and contemporaneous sedimentary processes. Therefore 3D seismic surveys are required to untangle the complex fault structures, quantify the distribution of sediments, and determine fault activity. Given the active tectonics and high earthquake density in this densely populated region, obtaining these datasets is critical to understand both geological evolution and associated hazards. The 3D seismic survey analysed in this work was primarily designed for exploration of hydrocarbons. It is the first dataset in the area to be released for research purposes. It covers part of the central northern Upper Rhine Graben (NURG), an area that shows the highest subsidence rates in Quaternary times (Ellwanger et al., 2005; Gabriel et al., 2013) and neotectonic fault activity (Peters and van Balen, 2007; Barth et al., 2015; Mair et al., 2025).

https://doi.org/10.5194/egusphere-2026-1626
Preprint. Discussion started: 15 April 2026

1.1 Geological Setting

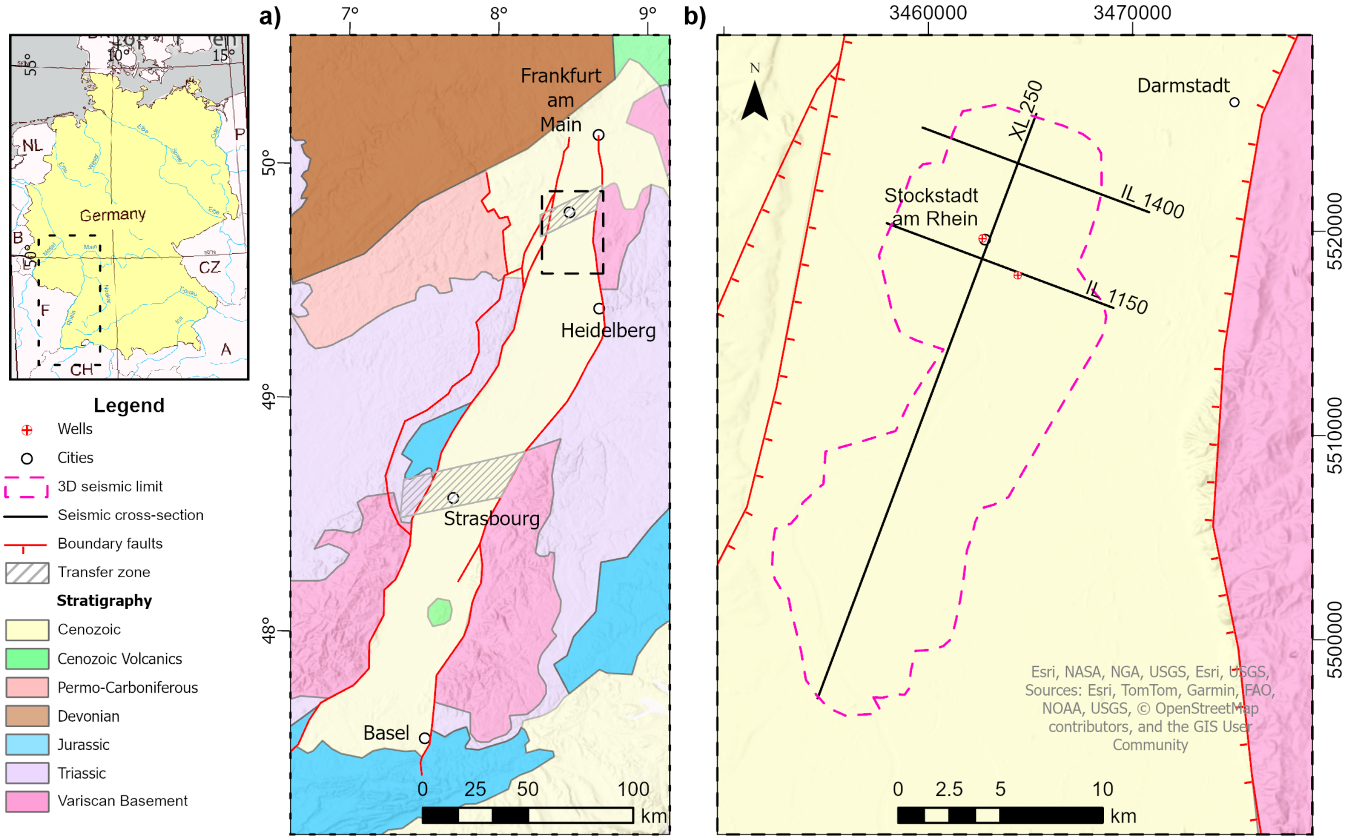

Figure 1. Location map of the Upper Rhine Graben and the study area (dotted black rectangle). Modified after Schumacher (2002a): a) simplified geological map of the URG, showing major bounding faults as red lines and transfer zones in grey slanted lines (Derer et al., 2005). b) Location of the 3D seismic survey (dashed magenta polygon). The position of the inlines and cross-lines shown in Figure 3 are marked in solid black line. Basemap Sources: Esri, TomTom, Garmin, FAO, NOAA, USGS, ©OpenStreetMap contributors, and the GIS User Community | Powered by Esri.

The crystalline basement of the URG was formed during the Late Paleozoic by the Variscan orogeny (Franke, 2000). This pre-existing structural grain, oriented predominantly NE–SW to NNE–SSW, has significantly influenced the Permian Rotliegend troughs as well as subsequent Mesozoic and Cenozoic evolution of the region (McCann et al., 2006).

1.2 Stratigraphy of the Northern Upper Rhine Graben

The stratigraphic succession in the NURG encompasses a wide range of lithologies, reflecting changes in depositional environments throughout the Cenozoic (Fig. 2). Units below the base of the Paleogene succession vary laterally and longitudinally, including basement and Rotliegend successions (Sissingh, 1998). Overlying sequences comprise fluvial, lacustrine, brackish, and marine deposits. The stratigraphy described here focuses on the main lithostratigraphic units.

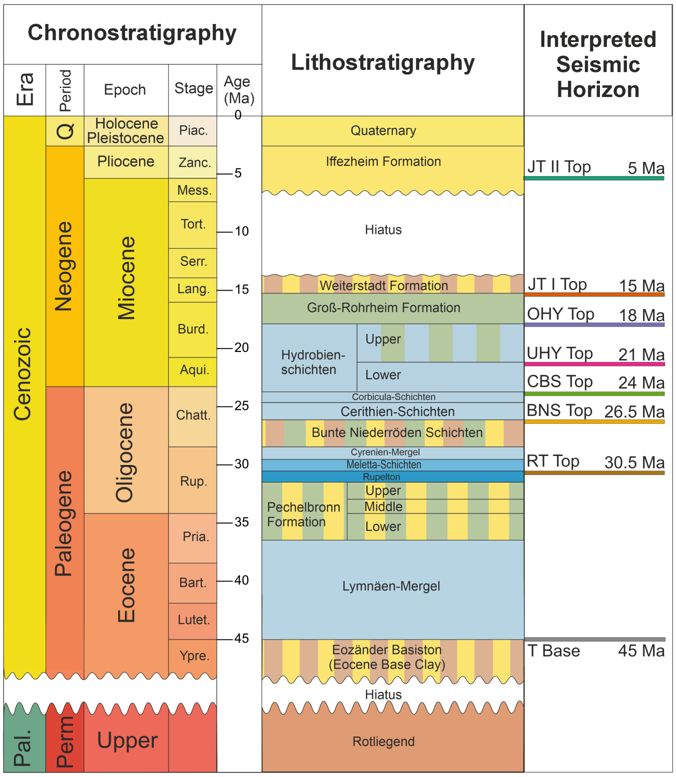

Figure 2. Chronostratigraphic and lithostratigraphic framework of the NURG, modified after Reinhold et al. (2016) and showing the position of the interpreted horizons.

- **Basement rocks**: Coarse-grained granodiorites of the Bergsträßer-Odenwald Group form the Paleozoic basement. These hard, low-carbonate, medium-grey rocks were encountered in the Stockstadt-33R well at approximately 2244 m (MD).
- **Rotliegend**: Composed of sandstones and siltstones, the Rotliegend represents a pre-rift unit formed under arid to semi-arid conditions, predominantly characterized by fluvial and aeolian facies (Schwarz and Henk, 2004; Becker et al., 2012).
- **Eocene Basal Clays (Eozäner Basiston)**: These red, highly weathered clays are associated with the early basin fill and exhibit marked lateral and vertical facies variations (Grimmer et al., 2017; Derer, 2003; Doebl and Teichmueller, 1979). The seismic top is named as T Base.
- **Lymnae Marl (Lymnäen Mergel)**: Known from the western NURG, this marl sequence was not directly encountered in local wells, but correlations from geophysical logs suggest its possible presence (Straub, 1962).

- **Pechelbronn Formation (Pechelbronn-Schichten — PBS)**: A sequence of Late Eocene to Early Oligocene fluvial to lacustrine sediments, subdivided into Lower, Middle, and Upper intervals, reflecting environmental changes during basin development.
- **Rupelian Clay (Rupelton — RT)**: Representing a transgressive event during the Late Rupelian, this open-marine shale is a prominent marker horizon (Reinhold et al., 2016).
- **Coloured Niederröder Beds (Bunte Niederrödern Schichten — BNS)**: Chattian limnic-fluviatile sediments that document further shift towards a terrestrial depositional environment.
- **Corbicula Beds (Corbicula-Schichten — CBS) and Hydrobia Beds (Hydrobia-Schichten — HYS)**: Oligocene to Miocene deposits ranging from marine to brackish. They are further subdivided (e.g., Lower and Upper Hydrobia Beds, UHY and OHY, resp.) which reflect environmental gradients.
- **Groß-Rohrheim Formations ("Jungtertär I", JTI)**: Burdigalian freshwater sediments that indicate a predominance of fluvial depositional systems.
- **Iffezheim Formation ("Jungtertär II", JTII)**: Pliocene sands representing continued sedimentation in predominantly continental settings.

Quaternary deposits, which reach thicknesses of up to 300 m near Heidelberg, consist mainly of fluvial sediments derived from the Neckar, Rhine, and Main rivers (Gabriel et al., 2013; Becker and Reischmann, 2021; Hoselmann and Lehné, 2012). These young deposits reflect ongoing sediment supply and basin fill under current environmental conditions.

1.3 Structural Framework

The URG is a prominent, north-northeast-trending segment of the ECRIS, extending from Basel in the south to Frankfurt in the north (Schumacher, 2002a; Derer et al., 2005; Frey et al., 2022b, a; Grimmer et al., 2017; Rotstein et al., 2005, 2008). The graben is typically subdivided into southern, central, and northern segments, with the NURG defined as the region north of the Ludwigshafen hinge zone (Bauer et al., 2025). Variations in sediment thickness and facies distributions are common and are influenced by local accommodation space and substrate properties. Growth faults and associated fault-block rotations, as identified in seismic data, delineate the internal configuration of the NURG and provide a framework for the observed sedimentary units (Rotstein et al., 2005).

The structural architecture of the NURG is the result of the interaction of pre-existing basement fabrics with subsequent rift-related deformation. The study area is located in the NURG in Germany (Fig. 1). While the structural complexity and fault network of the URG are partially well documented, interpretations of stress history and deformation phases vary. Some studies favour a long-lived sinistral transtensive regime (Cardozo and Behrmann, 2006b), while others propose multiple stress phases that have influenced fault patterns and basin geometry (Schumacher, 2002a; Rotstein et al., 2005; Frey et al., 2022b). Details of these interpretations are subject to ongoing research and will be addressed in the discussion section.

https://doi.org/10.5194/egusphere-2026-1626
Preprint. Discussion started: 15 April 2026

2 Data and Methods

The interpretation and modeling were carried out using the Petrel software of SLB. A Petrel project incorporating 3D seismic data, a velocity model, and the available well data was created. The interpretation was carried out with the *Seismic Interpretation* module, and the geological model was built using the *Structural Framework* module.

2.1 3D Seismic Data and Well Data Integration

The 3D seismic survey covers an area of approximately 10 km × 30 km between Worms in Rhineland-Palatinate and Darmstadt in Hesse, Germany. It was acquired by Rhein Petroleum GmbH between October 2011 and March 2012 for petroleum exploration. The data have only recently been made public under a new German law and are available via the Hessian Agency for Nature Conservation, Environment, and Geology (HLNUG). The seismic survey employed a 10–96 Hz sweep, with a shot and receiver spacing of 40 m, a sample interval of 2 ms, and a record length of 6 seconds. Since a proprietary velocity model was not available, interval velocities (V_{int}) were derived directly from the provided time-migrated and depth-converted horizon grids. For the target stratigraphic interval between the Upper Hydrobia Beds (OHY) and the Corbicula Beds (CBS), calculated interval velocities range from 2006 m/s to 2230 m/s. Based on these local velocity constraints and a dominant frequency of $\approx$ 60 Hz, the theoretical vertical resolution ($\lambda/4$; (Yilmaz, 2001)) is estimated at 8.3 m to 9.3 m. Consequently, our stated horizon picking uncertainty of ± 10 m is a conservative estimate that accounts for the derived nature of the velocity field and local variations in signal-to-noise ratio. Lateral resolution is improved by migration, which collapses the Fresnel zone to approximately $\lambda/2$, resulting in a lateral resolution of roughly 30 m (Brown, 2011; Yilmaz, 2001). Crucially, the Expansion Index (EI; see below) analysis is a ratio of thicknesses (T_{down}/T_{up}), meaning systematic velocity errors largely cancel out. This makes the derived tectonic growth histories robust, even in the absence of a proprietary velocity model.

Pre-stack, time-migrated seismic data were used to interpret nine main seismic horizons corresponding to the key stratigraphic units described in the previous section (see Fig. 2). These horizons were correlated with well markers from the gas fields of Wolfskehlen, Stockstadt (STO33R), and Hähnlein. The interpreted horizons in time were then converted to the depth domain for geological modeling.

Well STO33R provides critical stratigraphic and lithological information. According to the well report, approximately 500 m of Rotliegend sediments (comprising conglomerates, sandstones, and claystones) were drilled, with the granodiorite basement encountered at 2244 m (MD). The Tertiary Base represents an unconformity, and the upper Rotliegend was not identified, likely due to erosion. Stratigraphic markers from well STO33R were used to calibrate seismic interpretations and enhance stratigraphic correlations across the study area. The correlation of lithostratigraphic markers with seismic horizons —particularly along Inline IL-1150— improved the accuracy of horizon picking and fault mapping. In a non-faulted section, well STO-M1, a deviated well, located approximately 3 km northwest of STO33R, was used to validate the correlation of CBS and BNS. The thicknesses of the CBS and BNS horizons were derived from well markers (185 m and 338 m, respectively) and correlated with depth thickness maps. Well STO-M1 is shown on the UHY depth structure map, and its well path is projected on to IL-1150 and XL-250 (see Fig. 3a).

https://doi.org/10.5194/egusphere-2026-1626
Preprint. Discussion started: 15 April 2026

Table 1 summarizes the interpreted seismic horizons and their picking characteristics.

Table 1. Summary of Interpreted Seismic Horizons and Picking Characteristics.

Horizon	**Description**	**Picking Characteristics**
JTII Top and JTI Top	Tops of the "Jungtertär II" and "Jungtertär I" formations.	Picked along troughs.
OHY Top	Top of the Upper Hydrobia Beds, marking a homogeneous unit.	Picked along peaks.
UHY Top	Top of the Lower Hydrobia Beds, near the Rußingen Formation; characterized by a bundle of reflectors due to low-porosity dolomites.	Picked along peaks.
Top CBS	Top of the Corbicula-Beds.	Picked along peaks.
Top BNS	Top of the Bunte Niederrödern Beds, appearing as a bundle of bright reflectors below the UHY horizon.	Picked along troughs.
RT Top	Within the Rupelian Clay, affected by tuning effects; serves as a key seismic reflector.	Picked along peaks.
Base Paleogene (T Base) = Top Rotliegend	Marks the unconformity at the base of the Tertiary sequence.	Picked at zero-crossings.
Top Basement	Difficult to identify due to weak seismic response.	Not prominent.

Three representative seismic sections in the depth domain (inlines IL-1150 and IL-1400, and crossline XL-250) show the subsurface structure and fault geometries (Fig. 3c, d, e). Well STO33R intersects inline IL-1150, permitting direct correlation between lithostratigraphic markers and seismic horizons.

In this study, seven faults were examined in detail and grouped into two main sets based on their orientation: a predominantly NNW–SSE striking set and a WNW–ESE striking set (Fig. 3a). The NNW–SSE striking set comprises five faults (labeled 1A to 1E, with 1A being the southernmost). Within this set, faults 1D and 1E are the two main structures, with lengths exceeding 15 km and 10 km, respectively. They subdivide the northern part of the study area into three main blocks—western, central, and eastern. The other faults in this set (1A, 1B, and 1C) are shorter (5–10 km) and are arranged in an en-échelon pattern in the southern part of the area. The WNW–ESE striking set includes two faults, labeled 2A and 2B, with 2A being the southernmost.

2.2 Geological Modeling and Thickness Mapping

Using the interpreted depth horizons and faults, a geological model was constructed to represent the subsurface architecture. The model accounts for stratigraphic relationships between horizons and their interactions with faults. True vertical thickness maps of the stratigraphic units were generated to analyze variations in thickness and their relationship to fault activity. The mapped units correspond to the intervals between interpreted horizons (e.g., JTI Top to OHY Top, OHY Top to UHY Top, etc.), as illustrated in Fig. 4. These thickness maps help identify areas of differential subsidence and sedimentation associated with fault movement.

https://doi.org/10.5194/egusphere-2026-1626
Preprint. Discussion started: 15 April 2026

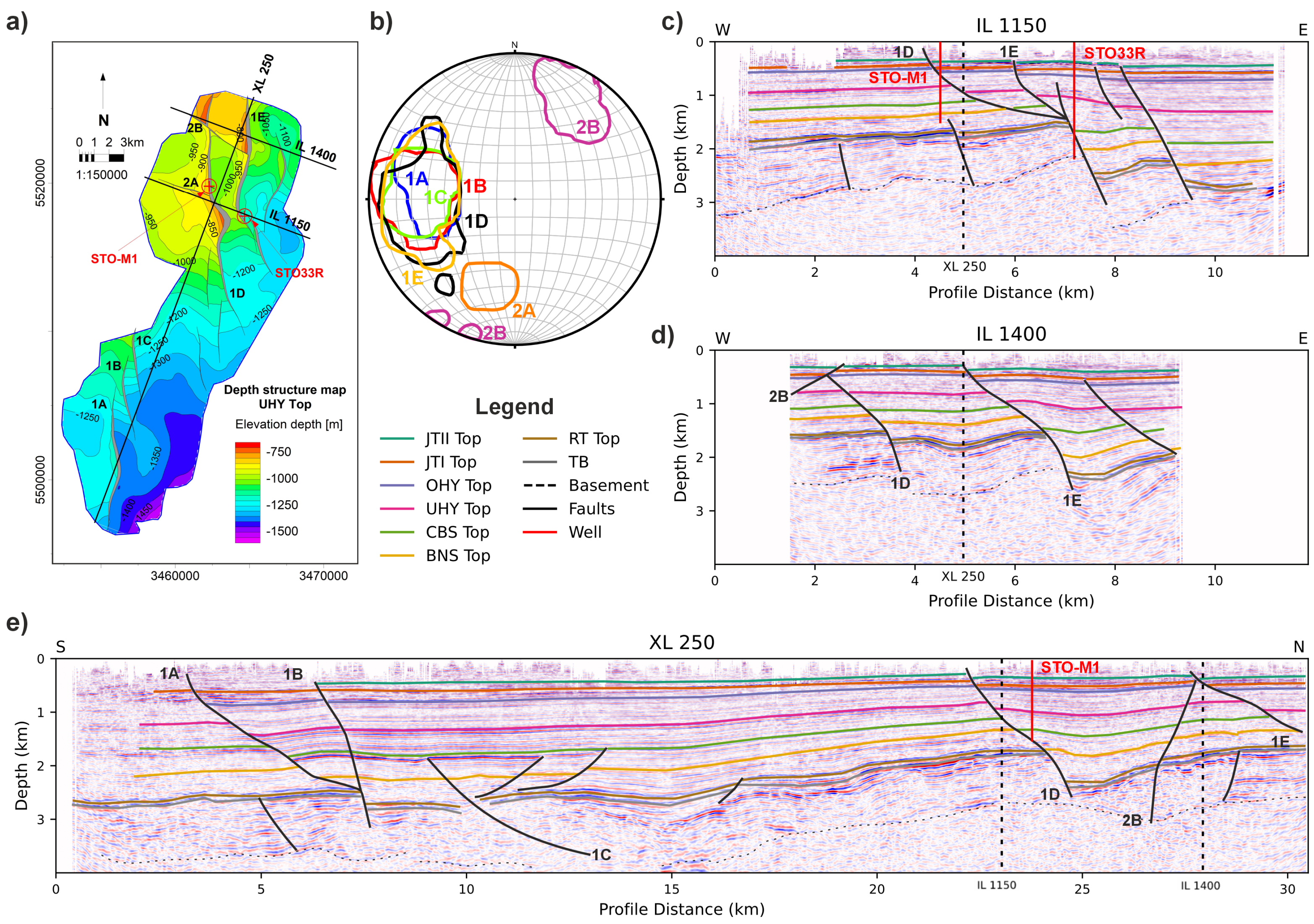

Figure 3. (a) Fault overview map at the top of the Lower Hydro Beds (UHY), displaying interpreted faults labeled 1A–E and 2A, B. (b) Equal-area stereographic projections of the lower hemisphere showing 1% isolines of poles to triangles that comprise the fault surfaces. (c–e) Seismic sections IL-1150, IL-1400, and XL-250 in the depth domain (2× vertical exaggeration). Section IL-1150 (c) illustrates Faults 1D and 1E in close proximity, merging at the RT Top level, while section IL-1400 (d) shows only Fault 1E remaining as a dominant structure at this latitude. STO33R is a vertical well; STO-M1 is a deviated well projected onto the seismic sections.

2.3 Geometrical Fault Shape Analysis

Fault surfaces were exported from Petrel as GoCAD triangulated surfaces (.ts files) to facilitate comparisons. In the Move suite from Petex, the strike and dip of the surface triangles were calculated and stored as attributes. The poles to these triangles were then plotted on a contoured equal-area stereographic projection with isolines at 1% of the uniform distribution density. The outlines of the 1% isolines for all faults were combined into a single stereographic projection (Fig. 3b).

2.4 Expansion Index and Activity Analysis

To quantify syn-sedimentary fault activity, we calculated the Expansion Index (EI), which is the ratio of the hanging-wall strata thickness (T_{down}) to that of the footwall (T_{up}):

$$\text{EI} = \frac{T_{\text{down}}}{T_{\text{up}}}$$

For a normal fault, an EI greater than one indicates differential subsidence and active faulting, while a value close to one implies limited or no syn-sedimentary fault movement (Childs et al., 2003; Pochat et al., 2009; Omosanya et al., 2015).

Uncertainty in the EI was calculated using standard error propagation, assuming a picking error of $\pm 10\,\text{m}$ for the thickness of each seismic horizon. This method accounts for the fact that the calculated uncertainty is largest for intervals with thin sedimentary thickness.

To compare fault activity both in terms of magnitude and timing, two metrics were visualized for each fault: the **absolute EI** and a **normalized EI**. The absolute EI allows for a direct comparison of the **magnitude** of activity between different faults. The normalized EI is used to compare the temporal evolution of **activity**, independent of magnitude. This normalization was achieved by dividing a fault's entire EI profile by its own lifetime maximum EI value, scaling its period of peak activity to 1.0.

All computations and visualizations were performed using Python-based workflows to ensure reproducibility. Both the absolute and normalized EI are presented as step plots versus age, with the calculated uncertainty shown as horizontal error bars. Scripts are available on GitHub repository (Mair, 2024).

https://doi.org/10.5194/egusphere-2026-1626
Preprint. Discussion started: 15 April 2026

3 Results

3.1 Fault Mapping and Seismic Cross-Sections

The interpretation of the 3D seismic data resulted in the identification and mapping of several faults within the study area. A fault overview map at the top of the Lower Hydrobia Beds (UHY) was generated (Fig. 3a) to display the interpreted faults. The faults are predominantly oriented in two main strike directions (one striking NNW–SSE and the other WNW–ESE).

Seismic cross-sections reveal that all identified faults exhibit normal displacement with varying throws across different stratigraphic levels. The faults extend from the basement through the Cenozoic sediments, indicating long-lived tectonic activity. The stereographic projection (Fig. 3) shows two predominant fault sets and the spread of strike and dip of individual faults.

3.2 Thickness Variations and Sedimentation Patterns

Analysis of sediment thickness maps (Fig. 4) reveals a general trend of increasing thickness from NW to SE, with significant local variations controlled by fault activity. These observations are quantitatively supported by the Expansion Index (EI) calculations for individual faults (Fig. 6).

JTI Top (14 Ma) – OHY Top (18 Ma): For this interval, thickness varies between 100 m and 210 m (Fig. 4a). A thicker accumulation is observed in the eastern fault block and notably in the southwest (hanging wall of Fault 1A). This corresponds to relatively low tectonic activity, with EI values on the major faults (1D, 1E) averaging ≈ 1.12 (Fig. 6d, e). This indicates that while sedimentation was continuous, differential subsidence across the major NNW–SSE faults was minor during this phase.

OHY Top (18 Ma) – UHY Top (21 Ma): Thicknesses range from 300 m to 660 m, averaging about 500 m (Fig. 4b). A prominent depocenter is evident near the eastern hanging wall (eastern fault segment of Fault 1E) . This asymmetry is captured by the EI analysis, where Fault 1E shows a distinct increase in activity, reaching an EI of ≈ 1.25 (Fig. 6e), effectively confirming that the eastern block was subsiding 1.25 times faster than the footwall.

UHY Top (21 Ma) – CBS Top (24 Ma): Thickness ranges between 300 m and 550 m (Fig. 4c). The eastern block dominance intensifies, with thickness increasing gradually toward the south. This interval marks the onset of significant extension, with EI values on Fault 1E rising to ≈ 1.60 (Fig. 6e), indicating that syn-sedimentary faulting was controlling nearly 40% of the accommodation space creation.

CBS Top (24 Ma) – BNS Top (26.5 Ma): In this interval, sediment thickness varies significantly (250–520 m), with notable "bullseye" maxima located directly adjacent to Faults 1D and 1E (Fig. 4d). This strong fault control corresponds to the peak of the rifting phase. Fault 1E records its maximum activity during this time, with a peak EI of 1.86 (Fig. 6e), while Fault 1D reaches an EI of ≈ 1.40 (Fig. 6d). This confirms that during the Chattian, the basin subsidence was primarily driven by the mechanical growth of these NNW–SSE faults.

BNS Top (26.5 Ma) – RT Top (30.5 Ma): Thickness ranges from 300 m to 500 m (Fig. 4e), with local thickening patterns similar to the overlying CBS interval. This is reflected in the EI analysis, where high EI values (>1.5) persist on the major faults, marking the early established phase of the graben subsidence.

https://doi.org/10.5194/egusphere-2026-1626
Preprint. Discussion started: 15 April 2026

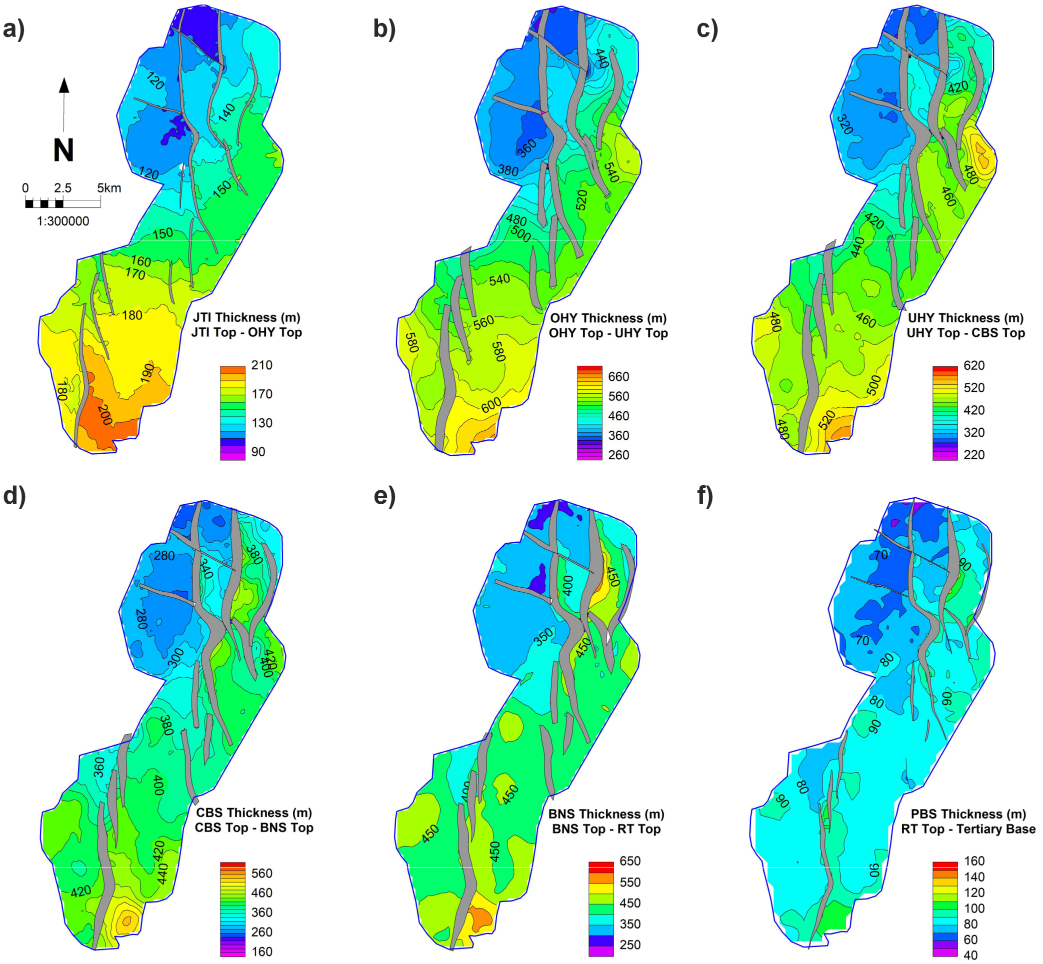

Figure 4. Thickness maps of various stratigraphic intervals. Note the increased sediment thickness (depocenters) in the hanging-walls of Faults 1D and 1E starting from the OHY interval (b). A southward migration of the maximum thickness is observed in the youngest interval (JTI, a), coinciding with the lateral propagation trends shown in the fault throw profiles.

3.3 Fault Throw Analysis

Fault throw profiles reveal that displacement is primarily concentrated on the major NNW–SSE striking faults (1D and 1E), while intersecting faults create zones of reduced throw, indicative of displacement transfer.

Fault throw measurements (Fig. 5) document vertical displacement along fault surfaces at various seismic reflector levels (see Fig. 3). While displacement was predominantly vertical during the early rifting stage, the profiles indicate a significant shift in growth style over time. Specifically, the NNW–SSE striking faults (1A, 1B, and to a lesser extent 1D/1E) exhibit a southward migration of displacement maxima in post-rift sequences. This transition from bell-shaped (radial) growth to

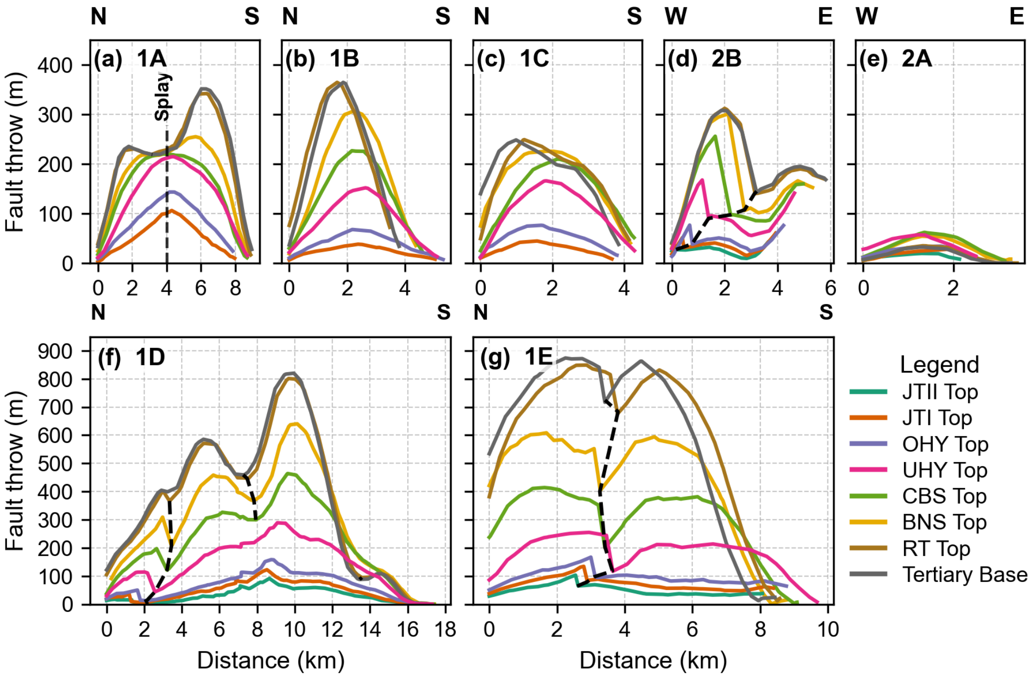

Figure 5. Fault throw profiles vs. strike length. Note the transition from bell-shaped (radial) growth in early stages to unilateral southward propagation in younger intervals. The profiles show a hard-linked splay on Fault 1A (at ≈ 4 km), merging with Fault 1B at the RT Top. Faults 1D and 1E also exhibit converging throw distributions at the RT Top level, consistent with the merging observed in seismic section IL-1150. Significant throw reductions are observed at fault intersections (e.g., Fault 1D/2B).

205 unilateral southward propagation suggests a directional “unzipping” of faults, consistent with the imposition of a sinistral shear component.

Crosscutting relationships further complicate the structural framework, where crosscutting interactions are marked as black lines in Fig. 5. Fault 1A is crosscut by Fault 1B; Fault 1D is dissected by Faults 2A and 2B; and Fault 1E is offset by Fault 2B. Notably, the intersection of Fault 1E and 2B exhibits a distinct “zig-zag” geometrical refraction with an offset of approximately 1 km. Further structural complexity is observed centrally, where Fault 1D coalesces with Fault 1E at the BNS stratigraphic level. Additionally, Fault 1A displays a hard-linked splay at approximately 4 km along its strike. Intersecting faults consistently reduce the throw on the host fault at the point of intersection; this effect is most pronounced where Faults 2A and 2B crosscut Fault 1D, and where Fault 2B crosscuts Fault 1E (Fig. 5).

Faults 1D and 1E record the largest cumulative vertical displacements. In contrast, Faults 1A–1C display smaller displacements and gradually change strike from N–S to NW–SE with depth (Reinhold et al., 2016). Stereographic projection analysis (Fig. 3b) confirms that Faults 1A–1C vary in strike orientation while maintaining consistently steep dips, i.e., they are helicoidal in shape.

3.4 Expansion Index and Fault Activity Timing

The temporal evolution of fault activity was analyzed using histograms of the Expansion Index (EI) versus stratigraphic age (Fig. 6). The **Absolute EI** (top panels, Fig. 6a–g) highlights the hierarchy of fault magnitude. The major NNW–SSE trending faults, **1D** and **1E**, accommodated the bulk of the extension, reaching peak EI values of approximately 1.86 during the deposition of the BNS and CBS units (Oligocene). In contrast, the minor NNW–SSE faults (1A–1C) and the WNW–ESE faults (2A, 2B) show significantly lower displacement magnitudes, with EI values rarely exceeding 1.25. While Fault 1A shows a decrease in activity toward the OHY horizon before reactivating, Fault 1C displays consistently low activity throughout.

The **Normalized EI** (bottom panels, Fig. 6h–n) decouples timing from magnitude to visualize the relative activity history. The quantitative implications of these trends are discussed in Section 4.2.

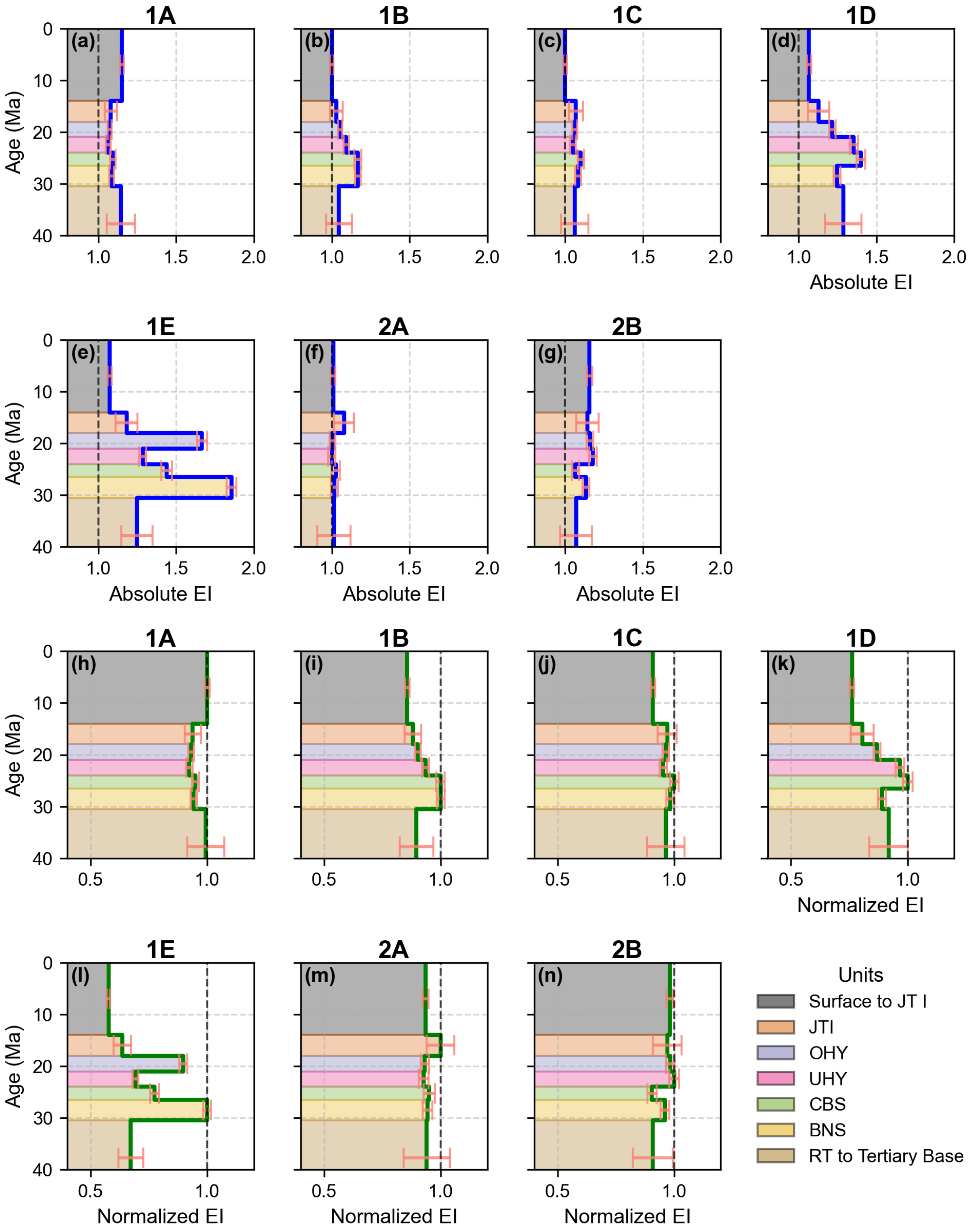

Figure 6. Temporal evolution of fault activity quantified by the Expansion Index (EI). **(Top)** Absolute EI (blue profiles) indicates that the major NNW–SSE boundary faults (1D and 1E) accommodated the majority of strain, peaking during the BNS and CBS intervals. **(Bottom)** Normalized EI (green profiles) reveals a clear kinematic decoupling: NNW–SSE faults peak during the early rifting stage (pre-24 Ma), whereas WNW–ESE faults (2A, 2B) show increased relative activity during the transtensional stage (post-24 Ma). This temporal divergence documents the activation of the transverse shear system.

https://doi.org/10.5194/egusphere-2026-1626
Preprint. Discussion started: 15 April 2026

4 Discussion

The integrated analysis of seismic data, thickness maps, and fault throw measurements reveals a complex tectonic history in the NURG. This history is characterized by the simultaneous activity of multiple fault sets, consistent fault propagation, significant fault interaction, and a marked tectonic regime shift (Cardozo and Behrmann, 2006b; Behrmann et al., 2005; Schumacher, 2002a). These factors have collectively influenced sedimentation patterns and the structural evolution of the basin.

4.1 Fault Propagation and Growth Histories

Faults within the study area exhibit consistent propagation styles throughout their history. They predominantly display normal faulting mechanisms from initiation to the present day, indicating that the basin underwent a prolonged extensional tectonic regime. Faults such as 1D and 1E demonstrate significant vertical displacement. Their early evolution appears consistent with the constant-length fault model (Childs et al., 2003), characterized by rapid establishment of fault length followed by displacement accumulation. However, the southward migration of displacement maxima observed in Faults 1A and 1B (see pronounced asymmetry in Fig. 5f, g) indicates a departure from this model during the Miocene. This unilateral southward propagation suggests that the imposition of the NW-SE transtensional regime facilitated the lateral ’unzipping’ of faults towards the south, modifying their original geometries.

4.2 Fault Interaction and Structural Relationships

The contemporaneous activity of both NNW–SSE and WNW–ESE striking fault sets is a notable feature of the NURG tectonic evolution. Faults 1D and 1E (NNW–SSE striking) and faults 2A and 2B (WNW–ESE striking) crosscut and were, for the most part, concurrently active, as evidenced by their throw patterns and structural relationships. We hypothesize that the minor faults 2A and 2B served as transfer structures up to the CBS horizon (∼24 Ma), accommodating displacement between the larger faults and facilitating strain transfer under extensional stresses.

The structural map of the UHY horizon (Fig. 3a) visually captures the interaction between the two tectonic phases. A prominent WNW–ESE structural high (characterized by shallow depths of -800 to -950 m) marks a distinct accommodation zone defined by Faults 2A and 2B. Crucially, the major NNW–SSE rift faults (1D and 1E) do not cross this zone undeflected; instead, they exhibit sharp geometrical refractions and terminations at this boundary. This spatial pattern confirms that the WNW–ESE faults were not merely passive pre-existing fabrics, but became kinematically active post-24 Ma, effectively dissecting the earlier rift geometry and forcing the NNW–SSE faults to kinematically reorganize under the new transtensional stress regime, as described by Bauer et al. (2025).

After deposition of the CBS, a shift in the tectonic regime led to a change in fault activity. Faults 2A and 2B began actively operating in parallel with the major faults, reflecting a reorientation of the stress field and a significant tectonic adjustment that influenced fault kinematics and interactions, while maintaining a normal fault regime. The distinct geometrical refraction (’zig-zag’ pattern) observed at fault intersections (e.g., Fault 1E and 2B) is interpreted as a mechanical response to this stress rotation. This refraction is not merely a passive geometrical feature; it is kinematically expressed by the increased activity of the transverse faults. Quantitatively, this is evidenced by the distinct kinematic divergence between the two fault sets: The NNW–SSE striking faults (**1A–1E**) consistently exhibit their peak relative activity (Normalized EI $\approx$ 1.0) during the older, rift-dominated intervals (Oligocene to pre-24 Ma), whereas the WNW–ESE striking faults (**2A** and **2B**) display a reverse trend, reaching their peak relative activity in the younger Miocene intervals (post-24 Ma; Figs. 6m, n). This temporal shift provides quantitative evidence that the WNW–ESE structures, while originating as passive transfer zones (Schumacher, 2002b; Derer et al., 2005), became kinematically active elements during the transition to the Miocene transtensional regime (Sissingh, 1998; Cardozo and Behrmann, 2006a).

Structurally, this segmentation is clearly visible in the seismic profiles (Fig. 3c–e), where the steep N–S faults are observed to mechanically link with the WNW–ESE segments, forming a continuous but refracted displacement surface that accommodates the oblique extension. We also note that Fault 1D and Fault 1E exhibit a complex interaction, effectively merging into a single kinematic linkage at the BNS/CBS stratigraphic level (approx. 3400 m distance). This merging coincides with a marked change in fault geometry closer to the basement, particularly for Fault 1D, where the deep (Tertiary) section is spatially decoupled from the shallow cover (offset by $>$ 1km). This decoupling further implies that the pre-rift structural grain exerted a strong control on the initial fault nucleation, which was arguably disparate, before the individual fault segments coalesced during the main extensional phase.

The seismic data reveals a significant structural transition at the RT Top level, where previously simple, basement-seated faults begin to diverge into complex splay systems (Fig. 3c–e). We interpret the Rupelian Clay (RT) as a critical rheological boundary within the Cenozoic succession (Cardozo and Behrmann, 2006b; Derer et al., 2005). Due to its ductile nature as an open-marine shale, the RT likely functioned as a mechanical decoupling layer (décollement). This rheological contrast allowed the high-magnitude strain localized on ancestral basement structures to be partitioned and distributed into multiple splay-like geometries within the overlying, more brittle stratigraphic units (Cardozo and Behrmann, 2006a; Bauer et al., 2025). The convergence of throw values for Faults 1D/1E and 1A/1B at this specific horizon (Fig. 5) physically documents this depth-dependent shift in deformation style (Mair et al., 2025).

4.3 Tectonic Regime Shift and Its Implications

We observe two distinct tectonic phases in our data, shown in Fig. 7: 1) pre-24 Ma, 2) post-24 Ma to the present-day. This concurs with other authors, such as Bauer et al. (2025); Cardozo and Behrmann (2006b); Behrmann et al. (2005); Schumacher (2002a).

4.3.1 Phase 1: Pure Rifting (Pre-24 Ma)

At the beginning of graben growth (pre-24 Ma), NNW–SSE striking faults (1D, 1E) prevailed with mainly normal displacement during BNS and CBS deposition. Syn-sedimentary thickness variations (250–520 m, 1:1.65 ratios near NNW–SSE faults) support this extensional model (Buchner, 1981; Behrmann et al., 2005). The regional stress field at that time showed a normal faulting regime with the maximum horizontal stress oriented NNE-SSW (Fig. 7).

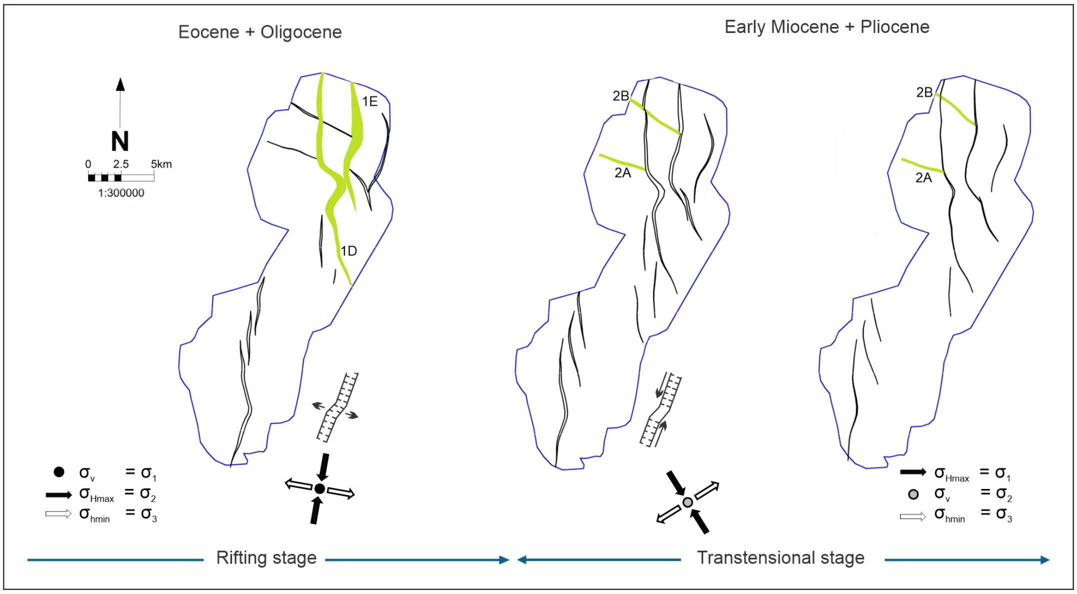

Figure 7. Tectono-sedimentary evolution model of the Northern URG. Left (Pre-24 Ma): Pure rifting stage. Strain is localized on N–S boundary faults (1D, 1E) under E–W extension (σ_3). Right (Post-24 Ma): transtensional stage. Rotation of σ_h to a NW–SE orientation triggers the activation and increasing kinematic relevance of WNW–ESE transfer faults (2A, 2B). The interaction between these sets creates the observed "zig-zag" geometrical refraction, where strain is partitioned between reactivated basement trends and new structures. Green shading highlights the locus of active subsidence derived from the EI analysis.

4.3.2 Phase 2: Transtension (Post-24 Ma)

After CBS deposition (∼24 Ma), the tectonic regime underwent a significant shift. Schumacher (2002a) have documented an anticlockwise stress-field rotation during this phase, which leads to a strike-slip regime with the maximum horizontal stress oriented NW-SE (Fig. 7). This is evidenced in our data by the activation of WNW–ESE oriented faults (2A, 2B) and the increase in their crosscutting behaviour with the earlier NNW–SSE structures. The observed "zig-zag" geometric refraction at the intersection of Fault 1E and 2B provides structural evidence for this stress rotation at approximately 24 Ma, marking the transition from pure extension to transtension. This fault geometry is characterized by a strong transversal shift at the southern end of Fault 1E, illustrating that the fault plane is more extended at the deeper section and changes shape significantly closer to the basement. This sharp geometrical change after the CBS horizon implies that the fault experienced at least two distinct episodes of movement. While such a strong offset forces a re-evaluation of simple planar geometry, it strongly supports the hypothesis of a separate, strike-slip-dominated movement phase that mechanically deformed the southern fault tips. The emergence of activity on these WNW–ESE faults reflects an increasing transtensional component, consistent with regional models that propose the Upper Rhine Graben acted in a sinistral fashion from the Pliocene onward, e.g. (Sissingh, 1998). This reorientation introduced strike-slip components to the previously dominant normal faulting regime.

While the major shift to transtension is often associated with the post-24 Ma interval, our data suggest that the Rupelian (RT) may mark the incipient phase of this reorganization. The onset of Alpine far-field stresses during the Middle Oligocene could have primed the existing N–S faults for the subsequent ’unzipping’ process. The RT Top thus represents a structural ’datum’ where the transition from deep-seated, simple faulting to a more distributed, transtensional fault network is first recorded.

In the modern configuration, the current stress regime (Dèzes et al., 2004), is characterized by simultaneous activity of both fault sets (Fig. 6; (Mair et al., 2025)). Vertical displacement acceleration since the Aquitanian (∼21 Ma) and the coexistence of extensional and strike-slip components highlight the influence of uplift and force redistribution tied to Alpine orogenic processes. These processes have modified fault kinematics and sedimentation patterns, culminating in the basin’s complex structural framework.

4.4 Influence of Fault Activity on Sedimentation Patterns

Active faulting has significantly influenced sediment deposition in the NURG. The quantitative correlation between fault throw and sediment accumulation provides conclusive evidence for syn-sedimentary tectonic control (Childs et al., 2003; Omosanya et al., 2015). While the PBS interval (pre-RT) shows relatively uniform thicknesses (80–100 m) with low EI values, the post-RT intervals (OHY and UHY) exhibit a dramatic increase in accommodation space. Specifically, sediment thicknesses escalate to over 600 m in the hanging walls of Faults 1D and 1E, directly coinciding with the peak Expansion Index (EI) values exceeding 1.60 (Mair et al., 2025). This simultaneous acceleration of vertical displacement and sediment flux confirms that the development of splay systems post-24 Ma was the primary driver for basin subsidence in the NURG (Kärcher, 1987; Bauer et al., 2025).

These thickness variations indicate differential subsidence and sedimentation patterns influenced by tectonic activity and fault movement. The presence of depocentre and local thickness maxima near faults suggests that faulting has played a significant role in controlling sediment accommodation space and deposition rates.

4.5 The URG as a Natural Laboratory for Oblique Rifting

While the sediment distribution confirms local subsidence trends, as described by Kärcher (1987) and Bauer et al. (2025), the structural observations from this 3D seismic volume have broader implications for rift mechanics globally. The NURG serves as a high-resolution natural laboratory for understanding how continental rifts respond to stress field rotation and structural inheritance.

4.5.1 Mechanical Response to Stress Rotation

Geometrical refraction—or “zig-zag” fault patterns—observed at the intersection of NNW–SSE and WNW–ESE faults is not unique to the Rhine Graben. This geometry is characteristic of “strain partitioning” in oblique rift settings, where new extensional stresses must be accommodated by reactivating older, misaligned basement fabrics.

https://doi.org/10.5194/egusphere-2026-1626
Preprint. Discussion started: 15 April 2026

Similar “zig-zag” boundary faults and distinct transfer zones have been documented in the East African Rift System (EARS), specifically where Cenozoic rifting interacts with Precambrian shear zones (e.g., Morley et al., 1990). However, unlike the EARS, where observations are often limited to 2D seismic or surface mapping, our 3D data physically resolves the linkage geometry at depth. We demonstrate that these “zags” (WNW–ESE faults) are not merely passive transfer zones but become active kinematic elements as the stress field rotates to transtension.

4.5.2 Spatial Evidence for the Unzipping Model

Our ’unzipping’ model is spatially validated by the observable change in fault linkage between the southern and northern parts of the study area (Sissingh, 1998; Mair et al., 2025). In seismic section IL-1150 (south), Faults 1D and 1E are observed in close proximity, effectively merging at the RT Top level into a single kinematic zone (Fig. 3c). Conversely, section IL-1400 (north) illustrates a distinct lateral separation, where 1D is significantly reduced in throw and 1E remains as the dominant, isolated structure (Fig. 3d). This transition from merged linkage in the south to structural divergence in the north represents a ’frozen’ record of the northward-opening fault system. This structural trend is further corroborated by the southward migration of sediment depocenters observed in the JTI thickness map (Fig. 4a), marking the late-stage activation of the southern fault tips under the Miocene stress regime (Bauer et al., 2025).

4.5.3 Implications for Multiphase Rifts

Consequently, the NURG model—characterized by early radial growth followed by late-stage unilateral propagation and geometrical refraction—offers a predictive template for other multiphase rift basins. It highlights that “complex” fault networks in the North Sea or Atlantic margins may not represent random fracture sets, but rather a deterministic mechanical response to rotating stress fields acting upon inherited crustal heterogeneity.

4.6 Present-Day Tectonic Activity and Implications

The basin remains tectonically active, with shear-wave seismic data documenting Quaternary base offsets exceeding 30 m (Mair et al., 2025). This high level of recent deformation contrasts with our Expansion Index analysis, which indicates a waning of fault activity toward the Late Miocene. This discrepancy suggests that the fault system did not follow a linear decline; instead, it underwent a distinct phase of tectonic acceleration or reactivation during the Quaternary. Consequently, the modern stress distribution is likely driven by this renewed pulse of activity rather than a continuation of earlier transtensional trends.

4.7 Implications for Geothermal Exploration and Natural Hazards

Understanding fault activity and sedimentation patterns is critical for geothermal energy exploration and seismic hazard mitigation. Active faults influence subsurface permeability and fluid flow, affecting the performance of geothermal reservoirs. Knowledge of fault growth histories and their spatial distribution can guide the optimal placement of geothermal wells while minimizing risks associated with fault reactivation. Furthermore, identifying regions of ongoing tectonic activity is essential for seismic hazard assessments, as differential movement of fault blocks can increase the likelihood of ground deformation and seismic events.

5 Conclusion

The integrated analysis of 3D seismic data, fault throw measurements, and sediment thickness mapping in the NURG reveals a complex Cenozoic tectonic evolution. Our findings identify a fundamental structural transition at the Rupelian (RT) level, where deep-seated, basement-linked faults splay into a more distributed network. This depth-dependent geometry defines the Rupelian Clay as a critical rheological decoupling layer that facilitated strain partitioning as the tectonic regime evolved.

The transition from pure rifting to transtension is structurally recorded by the geometrical refraction of fault intersection traces (the "zig-zag" effect) and the onset of unilateral southward fault propagation. This "unzipping" mechanism is physically evidenced by the spatial divergence of fault linkage, transitioning from merged fault zones in the south (e.g., IL-1150) to separated segments in the north (e.g., IL-1400). These 3D geometrical features provide robust physical evidence for the rotation of the regional stress field to a transtensional regime with the maximum horizontal stress oriented NW-SE post-24 Ma, corroborating the quantitative sedimentary evidence derived from the Expansion Index.

Episodic phases of enhanced fault activity during the Chattian and Miocene generated substantial accommodation space, creating localized depocenters. These results advance the understanding of Cenozoic fault dynamics in the Upper Rhine Graben and provide a structural framework for geothermal reservoir characterization and seismic hazard assessment. Future research incorporating high-resolution near-surface geophysical data is required to bridge the gap from the mid-Miocene to the documented Quaternary offsets.

Overall, the structural evolution of the Northern Upper Rhine Graben shows how rift systems respond to changes in regional stress fields over time. Our results indicate that the basin initially developed during a phase of pure extension, where NNW–SSE striking normal faults formed and accommodated most of the displacement during Oligocene rifting. Around $\sim$24 Ma, a rotation of the regional stress field led to the activation of WNW–ESE oriented faults, which had previously acted mainly as transfer structures. These faults became increasingly important and interacted with the earlier rift faults, producing the observed zig-zag fault geometries and a more complex fault network. At the same time, mechanical layering within the stratigraphy, particularly the ductile Rupelian Clay, influenced how deformation was distributed between deeper basement faults and shallower splay structures. Together, these results show that the evolution of rift basins is strongly controlled by stress field changes, pre-exisiting structures, and stratigraphic mechanical contrasts, which together shape fault growth and basin architecture through time.

Code Availability

The Python scripts used for the Expansion Index analysis and fault throw calculations are available in the GitHub repository (Mair, 2024).

Data Availability

The 3D seismic reflection data used for this study is available upon request under the respective German law (“Geologiedatengesetz”) from the Hessian Agency for Nature Conservation, Environment and Geology (HLNUG).

However, the interpreted fault surfaces and key stratigraphic horizons in the depth domain have been deposited in the GitHub repository (Roy, 2024) to ensure the reproducibility of the structural model as well as the verification of the reported fault intersection traces ("zig-zag" patterns) and throw profiles.

Author Contributions

SR, JM and AD produced the Petrel model and wrote the preliminary manuscript. All authors analysed the data and contributed to the manuscript.

Conflicts of Interest

No competing interests are present.

Acknowledgements

The authors thank the Hessian Agency for Nature Conservation, Environment and Geology (HLNUG) for providing the 3D seismic data and well data. We also thank MND Gas Storage Germany GmbH for providing 2D seismic lines and additional well data. We also acknowledge the use of Schlumberger Petrel educational licences. The study is part of the H2@Hessen project, funded by the Hessian Ministry for Economic Affairs, Energy, Transport, Housing and Rural Areas (Hessisches Ministerium für Wirtschaft, Energie, Verkehr, Wohnen und ländlichen Raum, HMWVW). The project is being conducted within the Engineering Geology group at the Institute of Applied Geosciences, TU Darmstadt, in collaboration with HLNUG.

References

Barth, A., Ritter, J., and Wenzel, F.: Seismicity and stress field of the Upper Rhine Graben (Central Europe), Tectonophysics, 665, 1–22, https://doi.org/10.1016/j.tecto.2015.02.018, 2015.

Bauer, F., Grimmer, J. C., Houpt, L., Hertweck, T., and Schill, E.: Development of intra-rift basins during stress field change in the central Upper Rhine Graben (SW Germany), Tectonics, 44, e2024TC008 721, https://doi.org/10.1029/2024TC008721, 2025.

Beccaletto, L., Capar, L., Cruz-Mermy, D., Oliviero, G., Elsass, P., Perrin, A., Rupf, I., Nitsch, E., and Tesch, J.: The GeORG project–seismic interpretation, structural pattern and 3D modeling of the Upper Rhine Graben–first scientific results, in: Technical workshop. Geopotential of the Upper Rhine Graben (GeORG).(Novembre 18th 2010, Freiburg (Germany).), 2010.

Becker, A., Schwarz, M., and Schäfer, A.: Lithostratigraphische Korrelation des Rotliegend im östlichen Saar-Nahe-Becken., Jahresberichte und Mitteilungen des Oberrheinischen Geologischen Vereins, 94, 105–133, 2012.

Becker, R. and Reischmann, T., eds.: Geologie von Hessen. Mit 300 Abbildungen, 2 Tafeln und 42 Tabellen., Schweizerbart, Stuttgart, ISBN 9783510654420, 2021.

Behrmann, J. H., Ziegler, P. A., Schmid, S. M., Heck, B., and Granet, M.: The EUCOR-URGENT Project, International Journal of Earth Sciences, 94, 505–506, https://doi.org/10.1007/s00531-005-0513-0, 2005.

Brown, A. R.: Interpretation of Three-Dimensional Seismic Data, AAPG Memoir 42, 7 edn., 2011.

Buchner, F.: Rhinegraben: Horizontal stylolites indicating stress regimes of earlier stages of rifting, Tectonophysics, 73, 113–118, https://doi.org/https://doi.org/10.1016/0040-1951(81)90178-5, mechanism of graben formation, 1981.

Cardozo, G. and Behrmann, J.: Kinematic analysis of the Upper Rhine Graben boundary fault system, Journal of Structural Geology, 28, 1028–1039, https://doi.org/10.1016/j.jsg.2006.03.010, 2006a.

Cardozo, G. and Behrmann, J.: Kinematic analysis of the Upper Rhine Graben boundary fault system, Journal of Structural Geology, 28, 1028–1039, https://doi.org/10.1016/j.jsg.2006.03.010, 2006b.

Childs, C., Nicol, A., Walsh, J. J., and Watterson, J.: The growth and propagation of synsedimentary faults, Journal of Structural Geology, 25, 633–648, https://doi.org/https://doi.org/10.1016/S0191-8141(02)00054-8, 2003.

Derer, C.: Tectono-sedimentary evolution of the northern Upper Rhine Graben (Germany), with special regard to the early syn rift stage, Ph.D. thesis, Bonn, Univ., Diss., 2003, 2003.

Derer, C., Schumacher, M. E., and Schäfer, A.: The northern Upper Rhine Graben: basin geometry and early syn-rift tectono-sedimentary evolution, International Journal of Earth Sciences, 94, 640–656, https://doi.org/10.1007/s00531-005-0515-y, 2005.

Dèzes, P., Schmid, S. M., and Ziegler, P. A.: Evolution of the European Cenozoic Rift System: interaction of the Alpine and Pyrenean orogens with their foreland lithosphere, Tectonophysics, 389, 1–33, https://doi.org/10.1016/j.tecto.2004.06.011, 2004.

Doebl, F. and Teichmueller, R.: Zur Geologie und heutigen Geothermik im mittleren Oberrhein-Graben, Forschungsarbeiten der Geologie von Rheinland und Westfalen, 27, 1–17, 1979.

Ellwanger, D., Gabriel, G., Hoselmann, C., Lämmermann-Barthel, J., and Weidenfeller, M.: The Heidelberg Drilling Project (Upper Rhine Graben, Germany), Quaternaire, 16, 191–199, https://doi.org/10.4000/quaternaire.406, 2005.

Franke, W.: The mid-European segment of the Variscides: tectonostratigraphic units, terrane boundaries and plate tectonic evolution, Geological Society, London, Special Publications, 179, 35–61, https://doi.org/10.1144/GSL.SP.2000.179.01.03, 2000.

Frey, M., Bär, K., Stober, I., Reinecker, J., van der Vaart, J., and Sass, I.: Assessment of deep geothermal research and development in the Upper Rhine Graben, Geothermal Energy, 10, https://doi.org/10.1186/s40517-022-00226-2, 2022a.

https://doi.org/10.5194/egusphere-2026-1626
Preprint. Discussion started: 15 April 2026

Frey, M., van der Vaart, J., Bär, K., Bossennec, C., Calcagno, P., Dezayes, C., Sass, I., and TU Darmstadt: Geothermal Resource Model of the Northern Upper Rhine Graben Crystalline Basement, https://doi.org/10.48328/TUDATALIB-898, 2022b.

Gabriel, G., Ellwanger, D., Hoselmann, C., Weidenfeller, M., and Wielandt-Schuster, U.: The Heidelberg Basin, Upper Rhine Graben (Germany): A unique archive of Quaternary sediments in Central Europe, Quaternary International, 292, 43–58, https://doi.org/10.1016/j.quaint.2012.10.044, 2013.

Grimmer, J. C., Ritter, J. R. R., Eisbacher, G. H., and Fielitz, W.: The Late Variscan control on the location and asymmetry of the Upper Rhine Graben, International Journal of Earth Sciences, 106, 827–853, https://doi.org/10.1007/s00531-016-1336-x, 2017.

Hoselmann, C. and Lehné, R.: Die quartärgeologische Entwicklung und ein geologisches 3D-Modell des nördlichen Oberrheingrabens, Geologisches Jahrbuch Hessen, 136, 77–88, 2012.

Kärcher, T.: Beiträge zur Lithologie und Hydrogeologie der Lockergesteinsablagerungen (Pliozän, Quartär) im Raum Frankenthal, Ludwigshafen, Mannheim, Speyer, Jahresberichte und Mitteilungen des Oberrheinischen Geologischen Vereins, 69, 279–320, https://doi.org/10.1127/jmogv/69/1987/279, 1987.

Mair, J.: NURG_Fault_Analysis, https://github.com/MairJ/NURG_Fault_Analysis, 2024.

Mair, J., Henk, A., Buness, H., Lehné, R., and Tanner, D. C.: Multi-scale geophysical imaging of neotectonic fault activity in the northern Upper Rhine Graben, Germany, Near Surface Geophysics, https://doi.org/10.1002/nsg.70013, 2025.

McCann, T., Pascal, C., Timmerman, M., Krzywiec, P., Lopez-Gomez, J., Wetzel, A., Krawczyk, C., Rieke, H., and Lamarche, J.: Post-Variscan (end Carboniferous–Permian) basin evolution in Western and Central Europe, Geological Society, London, Memoirs, 32, 355–388, https://doi.org/10.1144/GSL.MEM.2006.032.01.08, 2006.

Morley, C. K., Nelson, R. A., Patton, T. L., and Munn, S. G.: Transfer zones in the East African Rift System and their relevance to hydrocarbon exploration in rifts, AAPG Bulletin, 74, 1234–1253, https://doi.org/10.1306/0C9B2475-1710-11D7-8645000102C1865D, 1990.

Omosanya, K., Johansen, S. E., and Harishidayat, D.: Evolution and Character of Supra-Salt Faults in the Easternmost Hammerfest Basin, SW Barents Sea, Marine and Petroleum Geology, https://doi.org/10.1016/j.marpetgeo.2015.08.010, 2015.

Peters, G. and van Balen, R.: Pleistocene tectonics inferred from fluvial terraces of the northern Upper Rhine Graben, Germany, Tectonophysics, 430, 41–65, https://doi.org/10.1016/j.tecto.2006.10.014, 2007.

Pochat, S., Castelltort, S., Choblet, G., and Van Den Driessche, J.: High-resolution record of tectonic and sedimentary processes in growth strata, Marine and Petroleum Geology, 26, 1350–1364, https://doi.org/https://doi.org/10.1016/j.marpetgeo.2009.06.001, 2009.

Reinhold, C., Schwarz, M., and Perner, M.: The Northern Upper Rhine Graben: re-dawn of a mature petroleum province?, Bulletin f"ur angewandte Geologie, 21, 13–24, https://doi.org/10.5169/seals-658196, 2016.

Rotstein, Y., Behrmann, J. H., Lutz, M., Wirsing, G., and Luz, A.: Tectonic implications of transpression and transtension: Upper Rhine Graben, Tectonics, 24, https://doi.org/10.1029/2005TC001797, 2005.

Rotstein, Y. et al.: Tectonic implications of faulting styles along a rift margin: The boundary between the Rhine Graben and the Vosges Mountains, Tectonics, 27, https://doi.org/10.1029/2008TC002440, 2008.

Roy, S.: Horizon and Fault interpretation of NURG, https://github.com/sonuroy18/seismic_interpretation_NURG, gitHub repository, 2024.

Schumacher, M. E.: Upper Rhine Graben: Role of preexisting structures during rift evolution, Tectonics, 21, 6–1–6–17, https://doi.org/10.1029/2001TC900022, 2002a.

Schumacher, M. E.: Upper Rhine Graben: Role of preexisting structures during rift evolution, Tectonics, 21, 6–1–6–17, https://doi.org/10.1029/2001TC900022, 2002b.

Schwarz, M. and Henk, A.: Evolution and Structure of the Upper Rhine Graben: Insights from Three-dimensional Thermomechanical Modelling, International Journal of Earth Sciences, 94, 732–750, https://doi.org/10.1007/s00531-004-0451-2, 2004.

Sissingh, W.: Comparative Tertiary Stratigraphy of the Rhine Graben, Bresse Graben and Molasse Basin: Correlation of Alpine Foreland Events, Tectonophysics, 300, 249–284, https://doi.org/10.1016/s0040-1951(98)00243-1, 1998.

Sissingh, W.: Tertiary Paleogeographic and Tectonostratigraphic Evolution of the Rhenish Triple Junction, Palaeogeography, Palaeoclimatology, Palaeoecology, 196, 229–263, https://doi.org/10.1016/s0031-0182(03)00320-1, 2003.

Straub, E. W.: The petroleum and natural gas deposits in Hesse and Rhinehesse, Erd"ol am Oberrhein, 4, 123–136, publisher: Abhandlungen des Geologischen Landesamtes Baden-W"urttemberg, 1962.

Yilmaz, Ø.: Seismic Data Analysis: Processing, Inversion, and Interpretation of Seismic Data, Society of Exploration Geophysicists, 2001.

Ziegler, P. A.: European Cenozoic rift system, Tectonophysics, 208, 91–111, https://doi.org/10.1016/0040-1951(92)90338-7, 1992.